

ADVANCES IN CHARACTERISATION AND CALIBRATION OF DIGITAL IMAGING SYSTEMS

Horst A. Beyer

Institute of Geodesy and Photogrammetry

ETH-Hönggerberg, CH-8093 Zurich, Switzerland

phone: +41 1 377 3042; fax: +41 1 372 0438; e-mail: horst@p.igp.ethz.ch

Commission V

ABSTRACT

Real-Time Photogrammetry is making inroads into various applications due to its ability for on-line and real-time response. This opens applications in industrial measurement, robotics, traffic, medicine, etc. The accuracy of these Real-Time Photogrammetric Systems is a primary requirement for a large number of tasks. It is thus of utmost importance to investigate the accuracy potential of digital imaging systems. The radiometric and geometric properties of all elements involved in image acquisition and information extraction must be investigated in order to locate sources of degradations. With respect to photogrammetric applications effects leading to a degradation of the accuracy of three-dimensional measurements are of primary interest, whereas purely radiometric and geometric deformations which have no effect and/or which can be modelled are not of concern. It is thus necessary to locate the origins of degrading factors and to quantify their effect on the accuracy of three-dimensional measurements. This paper deals in a first part with the analysis of the radiometric and geometric characteristics of a number of components. Their effects on the accuracy of photogrammetric are discussed. A three-dimensional accuracy test with a testfield is used to demonstrate the accuracy potential of off-the-shelf hardware. Some limitations found in the test are pointed out and potential improvements are discussed.

KEY WORDS: Calibration, Image Quality, Accuracy, Sensor, Digital Systems

1 INTRODUCTION

Digital imaging systems have become an important topic in Digital Close-Range Photogrammetry. The readily available data makes real-time and on-line processing possible. This capability has opened a wealth of new application areas. The accuracy of these systems plays amongst many requirements such as automation, robustness, flexibility, and user-friendliness a fundamental role.

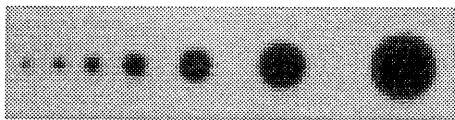
Real-Time Photogrammetry was already feasible with imaging tubes, but their low degree of stability limited their accuracy potential such that they did not gain widespread use in photogrammetric applications (e.g. Wong, 1969; Pinkney, 1978; Burner et al. 1985). The invention of the charge-coupled device in 1970 and the subsequent rapid development of solid-state imaging sensors, the commercial availability of flash analog-digital-converters, and the drastic performance increases of processing systems led to a dramatic change. The new sensors exhibited excellent characteristics and the processing systems allowed real-time feedback and/or the use of ever more demanding algorithms. Several characteristics, the accuracy, and the suitability of solid-state image sensors for Real-Time Photogrammetry were investigated among others by Gülch, 1984; Haggren, 1984; Curry et al., 1986; El-Hakim, 1986; Grün and Beyer, 1986; Wong and Ho, 1986; Dähler, 1987; Heikkilä, 1988; Lenz, 1988; Luhmann, 1988; Bösemann et al., 1990; Burner et al., 1990; Gustafson, 1991; and Shortis et al., 1991. Furthermore a wealth of knowledge on solid-state sensors, their characteristics, and performance was also acquired in astronomical and space tracking applications (see Beyer, 1992b for an extensive list of references). Pitfalls and the

performance of frame grabbers were also investigated (e.g. Raynor and Seitz, 1990).

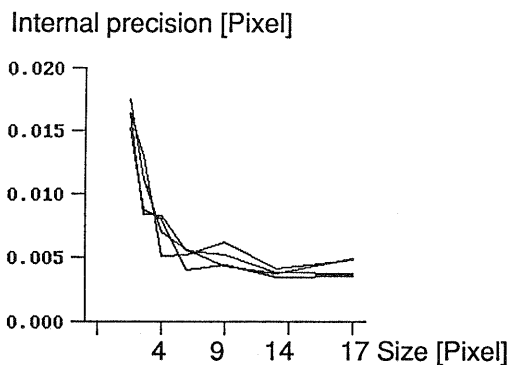
Building on this knowledge and expertise the radiometric and geometric characteristics of elements involved in image acquisition with solid-state imaging devices and their effect on the three-dimensional accuracy of photogrammetric measurements was investigated (Beyer, 1992a). Figure 1 shows the major elements of imaging and information extraction. The discussion shall be based on the assumption that the three-dimensional position of spatially limited features, such as signalized targets, are to be determined. This simplifies some evaluations but does not inhibit any generalization of the conclusions. The aim is thus to locate sources leading to geometric displacements of feature positions and/or to radiometric degradations decreasing the measurement precision and/or inducing geometric displacements.

First the characteristics of the elements are analyzed following the path of the data as shown in Figure 1. The influence of degrading factors on the accuracy of three-dimensional photogrammetric measurements is discussed. Synchronization, target size, temperature, and other effects are addressed and the inner precision of geometric measurements is investigated. Finally the performance of an off-the-shelf CCD-camera is investigated with a three-dimensional testfield. The effects of several degrading factors on the accuracy are analyzed. The performance of pixelsynchronous frame grabbing and PLL line-synchronization is compared. Limiting factors and potential improvements are discussed.

pixel is attained at latter diameter. This is only slightly improved for even larger targets to 0.004 pixel.



a) Targets



b) Internal precision of target location.

Figure 2 Analysis of internal precision as a function of target size.

The circle appears to be the best form for point positioning tasks as it is isotropic. If targets are allowed to cover large areas and the imaging scale is similar throughout the measurement range, targets with radially varying intensity can be used to increase the amount of gradients.

2.3 Optical Elements of Camera

Figure 3 shows an exploded view of the optical system of a typical CCD-camera. The radiometric and geometric

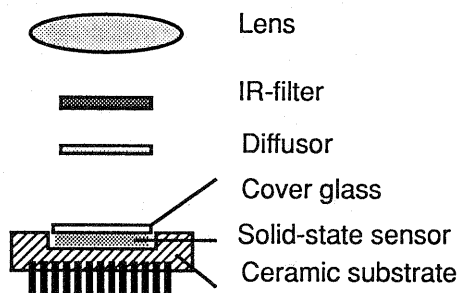


Figure 3 Functional elements of a solid-state camera.

characteristics of lens and optical system are well documented in literature. The geometric calibration of zoom lenses has also been addressed in recent years (e.g. Wiley and Wong, 1990). The fall-off of light to the corners induces radial displacements which are absorbed via parameters for radial symmetric distortion. The purpose of the IR cut filter was already explained. The diffusor is often incorporated into cameras with Interline Transfer sensors as well as color-cameras. It reduces aliasing by generating a double image displaced by 1/2 the sensor element pitch. The cover-glass over the sensor serves as chemical and mechanical protection.

The modulation transfer function (MTF) of the optics must be adapted to that of the sensor. This is relatively unproblematic for typical sensors having spacings of 10 to 20 μm . Cameras employing the micro-positioning technique with pixel spacings of a few micrometers (spacing of the pixels of the generated image) require appropriately designed lenses (MTF and aberrations).

The IR-filter, diffusor and cover glass should have plane parallel surfaces which are normal to the surface of the sensor. This is not provided in most CCD-cameras, i.e. specifications are only rarely provided. The diffusor is usually akin to a thin sheet of plastic of rather instable nature. The stability of the assembly of optical elements and sensor is for most CCD-cameras questionable. A stable fixture of the sensor to the camera body as well as specifications of the location of the optical axis in the imaging plane, its orthogonality with respect to the sensor surface, and the planeness and parallelity of the surfaces of other optical elements are some of the items to be required in the specifications of off-the-shelf CCD-cameras. Furthermore the MTF, aberrations, and spectral characteristics should be given.

2.4 Sensor

Solid-state sensor exhibit excellent radiometric and geometric characteristics. The Photo Response Non-Uniformity (PRNU), the surface characteristics, and the regularity of the sensor element aperture and spacing are of special interest.

The dark signal non-uniformity (DSNU) and photo response non-uniformity (PRNU) can be used to assess the basic radiometric performance. From an analysis of the DSNU electronic and other disturbances, independent of any sensor illumination, can be detected. The PRNU can be used to gain an overall impression of the quality of the imaging system. Effects of light-fall-off, dirt, and other degrading factors do often have larger impact than the PRNU of the sensor itself. Basically a radiometric correction could be performed on a pixel by pixel basis to correct for DSNU and PRNU. It is at this point in time questionable whether or not any improvement can be attained as the PRNU of typical off-the-shelf CCD-cameras is already in the range of 1%. The dependence of the

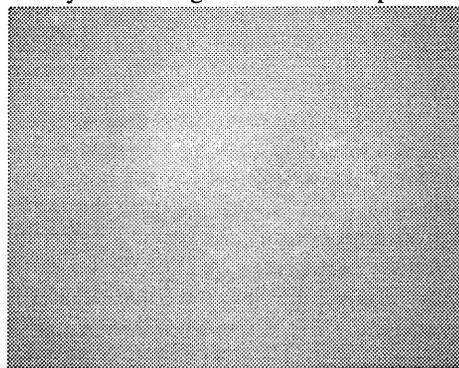


Figure 4 Photo response non-uniformity of a typical lens and camera.

PRNU on the spectral characteristics and the difficulty to generate a uniform illumination which is significantly better than 1% (Ulbricht spheres specify a uniformity of

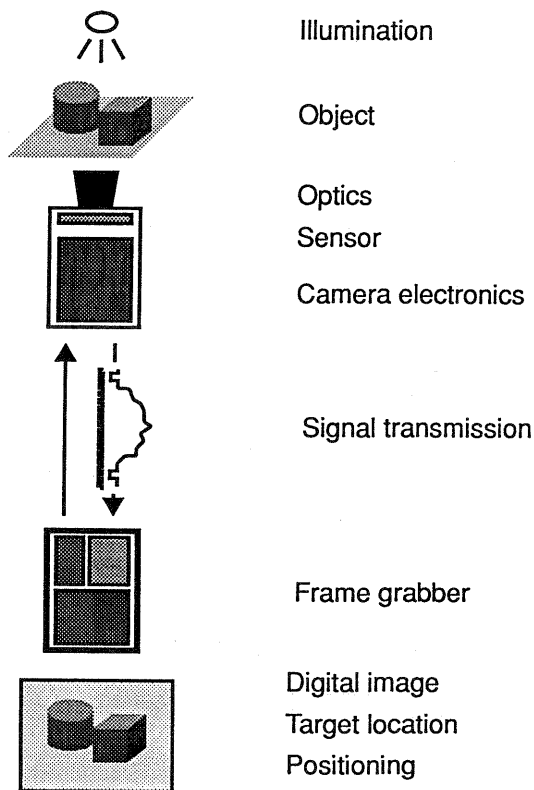


Figure 1 Image acquisition with solid-state imaging sensors.

2 CHARACTERISTICS OF COMPONENTS

2.1 Illumination

The importance of the illumination is generally underestimated. The temporal stability, the spectral characteristics, and the distribution of the light intensity on the object affect the measurement accuracy in several ways. The temporal stability is critical for very short, i.e. less than the power supply frequency, and very long image acquisition periods. Shuttered cameras (mechanical or electronic) need to be synchronized to the power supply of the lighting system when illumination sources which vary their light intensity with the frequency of the power supply are used. Electronically triggered fluorescent lights limit these variations to a few percent. Imaging systems requiring longer time spans for image acquisition, such as cameras with micro-displacement of the sensor (e.g. ProgRes 3000) or cameras with area and/or line sensors scanning a larger focal plane require an excellent long-term stability of the illumination for time spans ranging from several seconds to thirty minutes. The precise effect of the variation in illumination intensity on the accuracy depends on the type of sensor and the target location algorithm. When employing methods which are susceptible to illumination gradients across the area of features, e.g. centroiding or Least Squares Matching (LSM, Gruen, 1985), such variations must not induce illumination intensity gradients across the features. Ad-

joining pixels in imagery acquired with micro-positioning cameras will exhibit the variations over the complete acquisition time. Adjoining pixels of images acquired with line-scan cameras exhibit the variations occurring between the acquisition of individual lines.

The spectral characteristics of the illumination affect the photo response non-uniformity (PRNU) of the sensor as well as the modulation transfer function (MTF). The effect on the PRNU is considered to be negligible at this point as the PRNU of current solid-state sensors (produced for broadcasting applications) is better than 1% (see following discussion of PRNU). Optical crosstalk leads to a degradation of the MTF at longer wavelengths for front illuminated solid-state sensors. Many cameras do thus use an infrared (IR) cut filter to eliminate light with a wavelength longer than 800 nm, which has an absorption length (distance where 50% of photons were absorbed) of 10 μm in silicon.

The most obvious problem associated with the illumination is the variation of its intensity due to inherent properties of the illumination and/or shadows. Only the gradient induced across a feature of interest is of importance (Global differences do not lead to positional changes with typical target location algorithms like Least Squares Matching). Thus shadows, i.e. borders of shadows, are of great importance. Latter is dependent on the type of targets and illumination to be used. Shadows are a significant problem with standard targets but virtually nonexistent with retroreflective targets, which can in turn be affected by local variations in their reflectivity thus inducing similar problems (e.g. oily substances on retro targets). The different reflectivity of the surrounding areas of objects has also been found to lead to gradients of the illumination intensity on the object which can result in displacements of several hundreds of a pixel (Beyer, 1992a)

2.2 Object / Targets

The type, color, size, and form of a target do obviously affect the accuracy. Type (material) and color are factors defining the contrast of the target with respect to the background. Retroreflective targets exhibit the strongest return and can thus be used to provide the highest contrast. They can under certain conditions also exhibit more uniform reflective characteristics across the field of view as the degradation of the light intensity to the image corners due to the optical system can be counteracted via the stronger response as the angle between the illumination and the imaging rays becomes more optimal to the sides of the FOV (field of view), resulting in a stronger return. They are furthermore illuminated by lights on or close to the optical path of the camera, thus eliminating shadows.

The target size must be considered together with imaging scale. Figure 2 gives an empirically determined relation between the target size and the internal precision of target location. Figure 2 shows the targets ranging in diameter from 2 to 17 pixel. The diameter increases by a factor of $\sqrt{2}$ from target to target. The plot of the inner precision indicates the strong improvement for target diameters from 2 to 6 pixels. An internal precision of 0.005

better than 1%) indicate the problems. Furthermore only local slopes of the DSNU and PRNU across the area of targets will result in displacements of the target location. The total variation of the light fall-off due to the optical system and other influences is thus not relevant. Figure 4 shows the PRNU of a SONY-XC77CE camera with a 9 mm lens. The light fall-off to the corners and the irregularity of the grayvalues are apparent.

The subtraction of the thermal generated background (dark current) via the black reference is not always designed for highest accuracies. Several different variations exist which could potentially lead to very small deficiencies as the amount of dark current is already very small.

The sensor surface can exhibit global and local deformations as well as repetitive surface topography patterns. The global deviations have been found to reach 50 μm (Blouke at al., 1987). The surface topography of the sensor gates and other functional elements can reach several micrometers. The precise effect thereof on the location of image features as a function of the incidence angle is difficult to assess as the refraction coefficients of the various elements vary greatly and the precise location of the sensitive area of the sensor element depends on a number of factors. The displacements are not only a function of the radius from the image center but also of the direction, as structures exhibit row and column wise regularities. The advantages of this surface topography, as compared to film un-flatness, is that the displacement is stable in time and should thus be easier to determine. Figure 5 shows a cross-section of an Interline Transfer sensor. The elevated structure of the vertical CCD runs in columns direction and can be up to a few micrometer higher than the photodiode (light sensitive area).

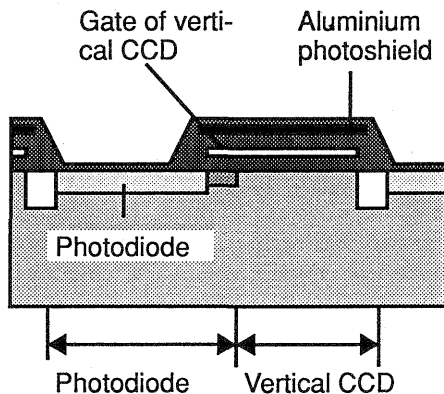


Figure 5 Cross-section through Interline Transfer sensor showing surface topography due to gate structure.

The regularity of the sensor elements can be assessed via the performance of the fabrication technology, actual measurements of the spacing, and the PRNU. All three sources allow to state that the regularity of the sensor element apertures and the spacing is better than 1%.

A review of sensor technology and their performance can be found in Beyer, 1992b and the extensive references therein.

2.5 Electronic Components of Camera

The electronic components of the camera serve to control the sensor, to perform analog signal processing, and to generate a video signal as well as other (synchronization) signals to be transmitted. Cameras with incorporated analog-to-digital converters, differ only with respect to the signal to be transmitted. The assessment of electronic components refers to off-the-shelf CCD-cameras produced as consumer products or for CCTV-applications (Closed Circuit Television).

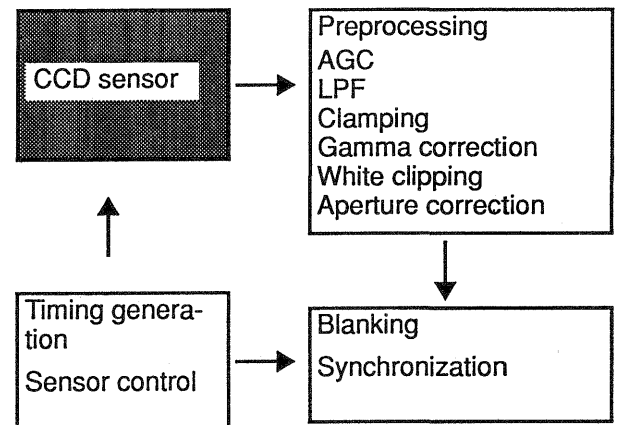


Figure 6 Block diagram of a typical CCD camera.

The analog preprocessing includes numerous signal processing schemes to enhance the signal-to-noise ratio and to eliminate electronic disturbances such as clocking transients from the sensor charge readout (e.g. correlated double sampling). Automatic gain control (AGC) assures a constant average image brightness with a feedback loop and signal amplification. This feature is helpful for human observation and certain applications but can induce unwanted intensity variations of features due to changes in other areas of the image (e.g. change of the background of an object). This can also be performed with a variation of the exposure time. The low pass filter (LPF) eliminates clocking transients and high frequency artifacts. They frequently exhibit an asymmetric impulse-response, reduce the MTF, and lead to ringing and a feature shift (e.g. Dähler, 1987; Lenz, 1988; see investigation of LPF of frame grabber). Clamping and white clipping limit the signal level to the video specifications. The analysis of temporal noise as a function of the gray-value can indicate another deficiency of a camera. It was found for several cameras that saturation is reached before the maximum video signal level is attained. Effects of gray level shift and a non-linear transfer function are only of relevance for radiometric analysis of the imagery and should not affect the three-dimensional measurement accuracy. Gamma correction compensates for the non-linear transfer function of TV-monitors. It destroys the excellent linearity of the sensor and should thus not be used if a linear transfer function is required. Aperture correction serves to improve the MTF, but eventual aliasing components will be enhanced as well. Contour correction, similar to an edge filter is included to enhance the visual impression, but can lead to degradations which are similar to those of the LPF.

The synchronization and blanking signals are added during signal generation. It was found that some information may be lost as the time available during the active image period is insufficient to submit the complete image data. Furthermore it was found that some pixels on the border are significantly darker, assumed to originate from the signal mixing. The synchronization signals must be derived from a master clock to enable a stable locking of the frame grabber onto the video signal (Beyer, 1988; Baltasvias et al., 1990).

2.6 The Frame Grabber

Frame grabbers do often include a multitude of processing capabilities. The following discussion is limited to functional elements involved in image acquisition from monochrome imagers.

Figure 7 shows the major functional elements of a frame grabber. The analog front end includes the impedance matching circuitry, the DC-restoration, analog offset, and analog gain control. Proper impedance matching is re-

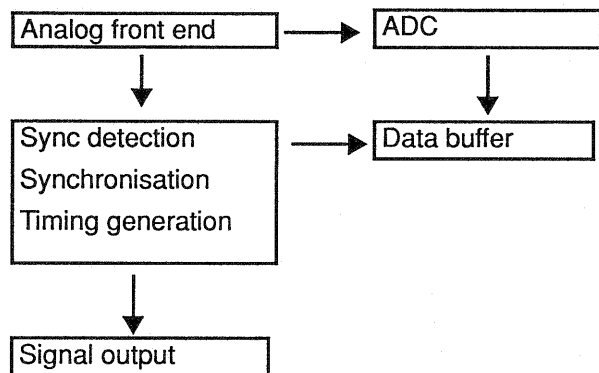


Figure 7 Typical image acquisition components of a frame grabber.

quired to circumvent signal reflections. DC-restoration removes the blanking level from the video signal. The location in time of the blanking signal and the quality and stability of the subtraction have been investigated. Wrong timing of the blanking signal sampling was found to lead to a variation of the subtracted signal level of over 4 grayvalues within up to 100 lines. This can induce a geometric displacement similar to local illumination gradients. The fall-off of the sample-and-hold mechanism used in many DC-restoration circuits was found to result in a uniform change of the background which can be disregarded. This small variation can be seen in Figure 8 as a slow increase of the image brightness from left to right.

The temporal noise characteristics of the frame grabber have been shown to be close to the theoretical limit of the analog-to-digital converter. More problematic are systematic patterns such as those shown in Figure 8. The origin of both the horizontal bands and the periodic phase patterns running at an angle of 45° could not be deter-

mined. They are assumed to originate from the host com-

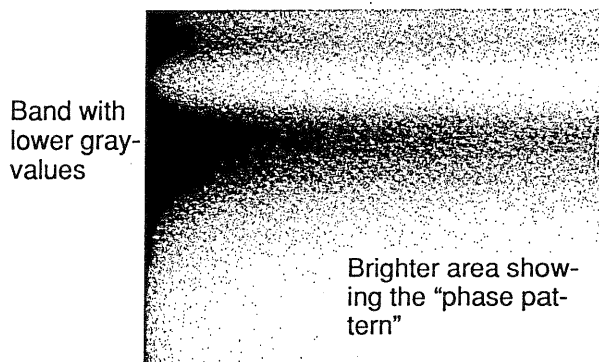


Figure 8 Average frame showing typical patterns of the frame grabber.

puter and other electronic components as they depend on the frame grabber board and its position in the chassis. The observed patterns can lead to displacements similar to those of local illumination gradients. The displacements from the "phase pattern" are dependent on the size and location of the target with respect to the pattern. The maximum influence was estimated to reach several hundredth of the pixel spacing as the peak-to-peak variation of the phase pattern is 4 to 6 grayvalues.

A strong integral non-linearity of the frame grabber was detected and appears to be typical for many frame grabbers. It must be considered when performing radiometric corrections and radiometric operations but is of no importance when considering the position of circular targets.

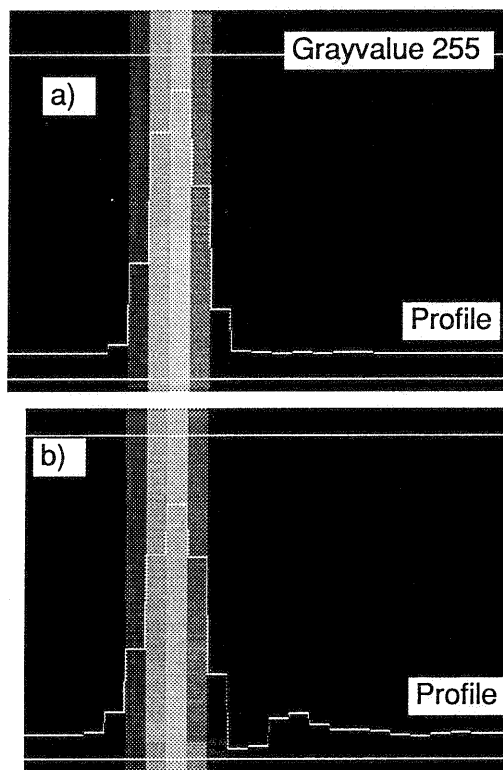


Figure 9 Image of a vertical line without and with LPF showing the asymmetric impulse response and ringing when the LPF is used (b).

The impulse response and the modulation transfer function of the frame grabber, especially of the low-pass-filters which might not be adapted to the signal frequencies, have several effects. On one hand the location of features will be displaced due to the asymmetric impulse response. Furthermore the internal precision will be degraded as the contrast of (small) targets is degraded due to the reduction of the MTF. Figure 9 a shows an image of a vertical line acquired with a MAX-SCAN frame grabber without its selectable LPF. Figure 9 b shows the same image acquired with the LPF. The asymmetric impulse response and the ringing are evident.

A factor with significant importance is the performance of the synchronization. Figure 10 shows the position of a line in imagery acquired with PLL line-synchronization (Figure 10 a) and with pixelsynchronous sampling (Figure 10b). PLL line-synchronization can induce a geometric deformation (in first order a shear) reaching several tenth of the pixel spacing as well as linejitter. The shear can be eliminated when HSYNC and VSYNC signals are used for synchronization instead of the CSYN of composite video signals. Pixelsynchronous sampling reduces synchronization errors to below 0.005 pixel. Its stability is a factor of 20 better than for PLL line-synchronization via CSYNC signals. The random positional changes of linejitter can be eliminated by averaging whereas the geometric deformation cannot be eliminated through averaging. It can on the other hand be modelled by including a shear as additional parameter. It must nevertheless be expected that pixelsynchronous frame grabbing provides for a higher accuracy than PLL line-synchronization, whether or not that can be translated into a higher three-dimensional accuracy must be verified.

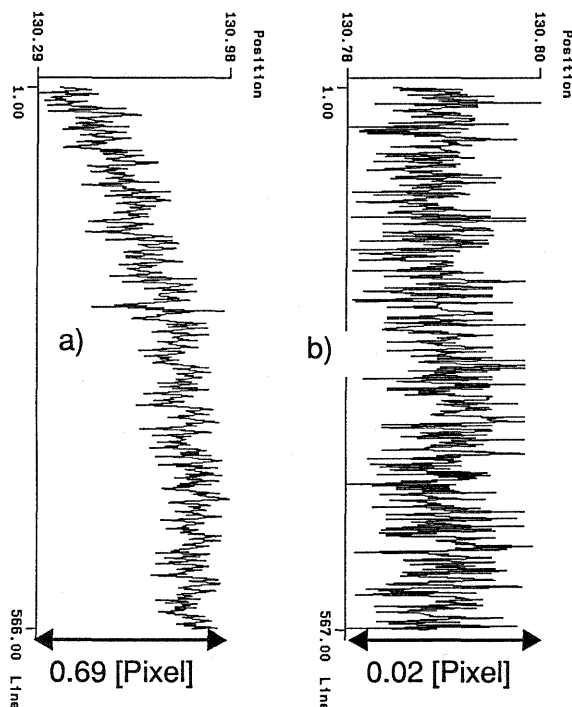


Figure 10 Position of a vertical line with PLL line-synchronization (a) and pixelsynchronous sampling (b).

2.7 Signal Transmission and Synchronization

Signal Transmission and synchronization are after temperature the factors leading to the largest radiometric and geometric disturbances. Image data transmission with digital signals and analog signals using PLL line-synchronization as well as pixelsynchronous frame grabbing were analyzed. It could be shown that the geometric performance of pixelsynchronous frame grabbing is identical to digital transmission and thus without loss. PLL line-synchronization leads in connection with the derivation of the frame grabber synchronization signals from a CSYNC signal to a shear reaching several tenths of pixels as well as linejitter. These effects were both determined via an investigation of the frame grabber and an investigation using MEGAPLUS and SONY-XC77CE cameras. It should be noted that linejitter does lead both to geometric and radiometric instabilities. Methods for the evaluation of the synchronization performance can be found in Beyer, 1988 and 1991.

2.8 Temperature

The temperature plays a significant role for the internal precision of measurements and such the accuracy to be attained. Warm-up-effects occurring after a camera, and to a lesser degree frame grabber, were switched on can lead to large variations in image positions. These were found to reach several pixels for PLL line-synchronization. For a SONY-XC77CE a displacement of 0.005 pixel in x and 0.1 pixel in y was detected within the first hour with pixelsynchronous frame grabbing. An internal stability of better than 0.01 pixel in x and y after a maximum of three hours could be verified for periods of several hours. The deformations occurring during warm-up with pixelsynchronous sampling are attributable to thermal deformations of the assembly. The larger variations observed with PLL line-synchronization are connected to variations of the clock frequency induced by the temperature change during warm-up.

2.9 Averaging

The internal precision of positioning can be improved by averaging. It was found that for pixelsynchronous sampling an improvement corresponding to theoretical expectations can be achieved for at least up to 5 frames. It could not be verified for longer sequences as the averaging was performed off-line and only 5 frames were acquired consecutively. If the time between series is several minutes other (electrical and mechanical) effects limit the improvement. It would thus be an advantage to use real-time averaging over a number of frames for applications where a stable configuration is given.

3 THREE-DIMENSIONAL ACCURACY

3.1 Testfield and Network

The three-dimensional accuracy of a SONY-XC77CE camera was investigated and verified using a three-dimensional testfield. The part of the testfield used in the test contains 162 targets placed on a wall and on 5 alu-

minium bars of a testfield structure. The targets span a volume of $2.6 \times 2.0 \times 1.1 \text{ m}^3$ (see Figure 12). The coordinate system is placed such that the X and Y axes are within the plane of the wall with the X-axis parallel to the floor and the Z axis points away from the wall. The coordinates of 86 targets were measured with theodolites both before and after the imagery for the test was acquired. The coordinates were determined with a precision of 0.02 mm in X and Y and 0.03 mm in Z. The targets are photographically produced black circles with a diameter of 20 mm on white background with a small white dot in the center for theodolite measurements. The centricity of the targets used for the theodolites is within 5 to 6 μm of those used for the CCD-cameras.

Figure 11 shows the testfield with camera, theodolite,

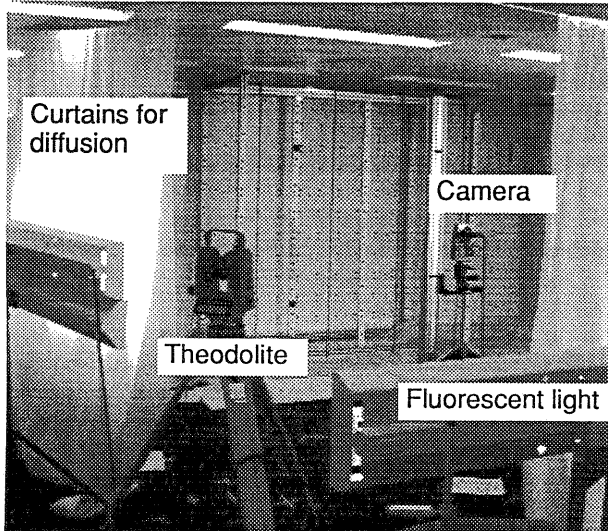


Figure 11 Testfield, illumination, camera, and theodolite.

lights and curtains. The lights and curtains were placed to generate a diffuse uniform illumination. The rods of the structure and the camera fixture create visually almost undetectable shadows on the wall. The local illumination gradients are stable for shadows from the rods of the testfield rods but vary their location for each position of the camera stands.

The network and testfield are depicted in Figure 12. Images were taken with a SONY-XC77CE camera equipped with a FUJINON 9 mm lens at 24 stations with a roll of zero and 90 degrees. Both pixelsynchronous frame grabbing and PLL line-synchronization was used, each generating a set of 48 frames. This allows to investigate the effect of the synchronization on the three-dimensional accuracy. The image size is 728×568 pixel with a spacing of $11 \mu\text{m}$ in x and y.

The image scale varies between 1 : 200 and 1 : 560. The targets are thus imaged onto 3.3 to 9 pixels (diameter between inflection points of grayvalue profile) when excluding geometric foreshortening and other degrading effects. The internal precision of the target location for this size was experimentally determined to be in the range of 0.005 to 0.01 pixel. The targets were imaged in 36 images on average.

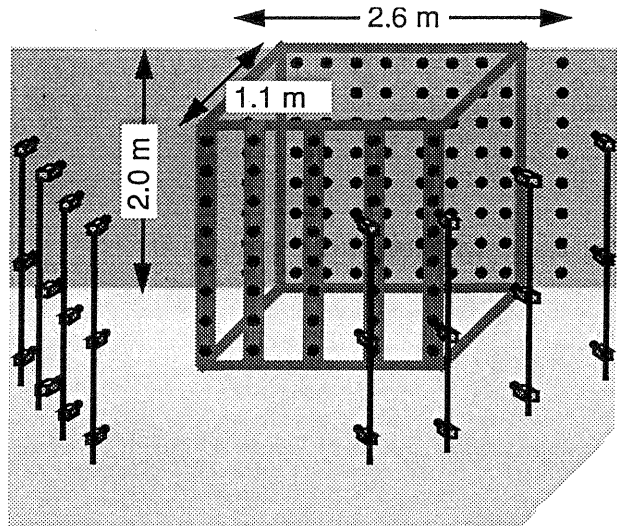


Figure 12 Testfield and camera network.

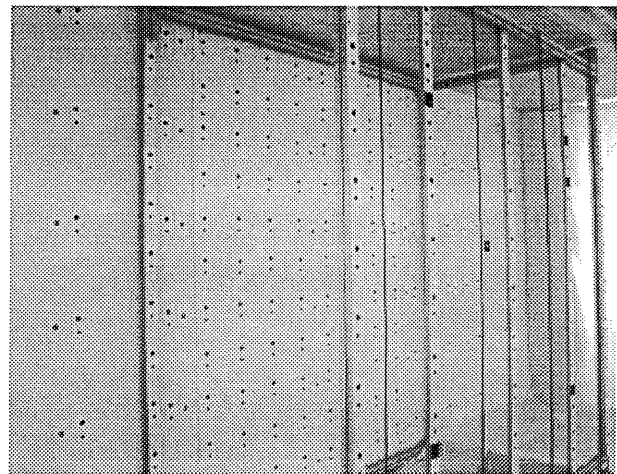


Figure 13 Image grabbed at leftmost station showing the large variation of image scale and the obliqueness.

3.2 Procedure and Mathematical Modelling

The pixel coordinates of all targets were measured semi-automatically with least squares matching (LSM). The pixel coordinates were subsequently transformed to pixel coordinates with the pixel-to-image coordinate transformation (see Figure 14 for the definition of the coordinate systems):

$$x = (x' - x'_p) \times psx \quad (1)$$

$$y = (y'_p - y') \times psy \quad (2)$$

with:

x, yimage coordinates

x', y'pixel coordinates

x'_p, y'_plocation of principal point in pixel

psx, psypixel spacing in x and y

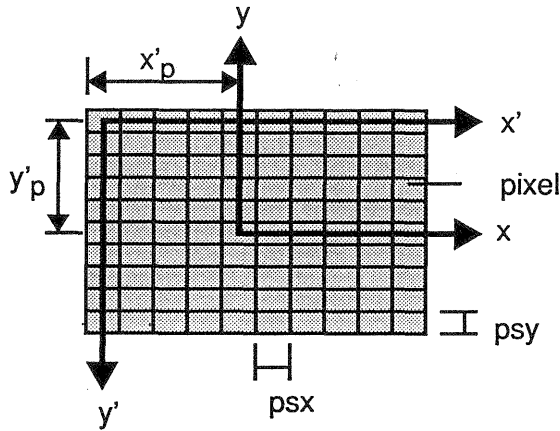


Figure 14 Pixel and image coordinate systems.

Additional parameters modelling the interior orientation, a scale factor in x, a shear, radial symmetric lens distortion, and decentering distortion was formulated as:

$$\Delta x = \Delta x_p - \frac{\bar{x}}{c} \Delta c - \bar{x} s_x + \bar{y} a + \bar{x} r^2 K_1 + \bar{x} r^4 K_2 + \bar{x} r^6 K_3 + (r^2 + 2\bar{x}^2) P_1 + 2\bar{x}\bar{y} P_2 \quad (3)$$

$$\Delta y = \Delta y_p - \frac{\bar{y}}{c} \Delta c + \bar{x} a + \bar{y} r^2 K_1 + \bar{y} r^4 K_2 + \bar{y} r^6 K_3 + 2\bar{x}\bar{y} P_1 + (r^2 + 2\bar{y}^2) P_2 \quad (4)$$

with:

$$\bar{x} = x - x_p, \quad \bar{y} = y - y_p, \quad r = \sqrt{\bar{x}^2 + \bar{y}^2} \quad (5)$$

$\Delta x_p, \Delta y_p, \Delta c$.change of interior orientation elements

s_x scale factor in x

ashear

K_1, K_2, K_3 first three parameters of radial symmetric distortion

P_1, P_2 first two parameters for decentering distortion

The location of the principal point is not specified for most CCD-cameras and varies from camera to camera and depends on the configuration of the frame grabber. The scale factor in x is required to model the imprecise specification of the sensor element spacing and additional imprecisions introduced with PLL line-synchronization. In latter case the pixel spacing in x must be computed from the sensor element spacing, the sensor clock frequency and the sampling frequency with:

$$psx = ssx \frac{f_{\text{sensor}}}{f_{\text{sampling}}} \quad (6)$$

with:

psx pixel spacing in x

ssxsensor element spacing in x

f_{sensor} sensor clock frequency

f_{sampling} sampling frequency of frame grabber

The shear (a) must be included to compensate for the geometric deformation induced by PLL line-synchronization as discussed above.

3.3 Accuracy with Pixelsynchronous Frame Grabbing

The results of several versions of bundle adjustments and accuracy verifications are given in Table 2. The large influence of the modelling of systematic errors is demonstrated with versions 1 and 2. Version 1 is computed with the initial values for the pixel-to-image coordinate transformation and the interior orientation and without additional parameters. The initial values of the pixel-to-image coordinate transformation (equations (1) and (2)) were derived from the camera and frame grabber specifications and settings. The camera constant was computed from the focal length and the focussing distance by the lens formula. Version 2 uses updated values for the transformation and the additional parameters of equations (3) and (4). The large improvement of the accuracy by factors reaching 70 is primarily due to the modelling of distortion. Table 1 gives the initial and adjusted values for the pixel spacing and the interior orientation elements. It can be seen that the changes to the pixel spacing and the camera constant are in this case rather small. The change in the location of the principal point corresponds to 3 pixel in x and 10 pixel in y. The precision of the location of the principal point and the camera constant are each determined with a precision better than one micrometer. The large distortion of the lens, exceeding 10 pixels at a radius of 3.6 mm, is apparent as a bending of the testfield rods in Figure 13.

Parameter	Initial value	Adjusted value	Standard deviation
Pixel spacing in x [mm/pixel]	0.011	0.0109995	0.0000036
Principal point in x [mm]	0.0	0.0323	0.00031
Principal point in y [mm]	0.0	0.1191	0.00025
Camera constant [mm]	9.0	8.9821	0.00018

Table 1 Initial and adjusted values of pixel spacing and interior orientation elements with their standard deviations (from version 2).

The results of version 2 indicate a large discrepancy between the theoretical precision estimates ($\hat{\sigma}_x, \hat{\sigma}_y, \hat{\sigma}_z$) and the empirical accuracy measures (μ_x, μ_y, μ_z). Large degradations were found to be due to local intensity variations. It was shown in an investigation that the effect of these gradients, due to shadows and differing reflectivity of surrounding areas of the testfield, could be decreased by using a smaller template (5 x 5 instead of 7 x 7). The results of these measurements are given in version 3. The accuracy in image space was thus improved by a factor of 1.3. The smaller template nevertheless only decreases but does not eliminate the effect of the local illumination gradients. It was thus decided to remove the targets with strong illumination gradients. This led to another improvement by factors up to 1.4 as indicated by the comparison of versions 3 and 4.

Version	AP	Co	Ch	r	$\hat{\sigma}_0$	$\hat{\sigma}_X$ [mm]	$\hat{\sigma}_Y$ [mm]	$\hat{\sigma}_Z$ [mm]	μ_X [mm]	μ_Y [mm]	μ_Z [mm]	μ_x [μm]	μ_y [μm]
1	0	30	56	11554	11.7	0.027	0.023	0.035	4.207	4.063	3.657	12.13	11.98
2	10	30	56	11547	0.36	0.027	0.023	0.035	0.086	0.058	0.114	0.24	0.22
3	10	30	56	11547	0.42	0.023	0.019	0.029	0.068	0.055	0.084	0.19	0.17
4	10	30	40	9879	0.42	0.023	0.019	0.028	0.062	0.039	0.056	0.16	0.14
5	10	30	38	8969	0.38	0.026	0.020	0.032	0.052	0.040	0.048	0.13	0.13
6	10	30	38	8963	0.46	0.033	0.025	0.039	0.056	0.039	0.061	0.14	0.14
<i>Improvement 1 / 2</i>					32.5	1.0	1.0	1.0	48.9	70.1	32.1	50.5	54.5
<i>Improvement 2 / 3</i>					0.9	1.2	1.2	1.2	1.3	1.2	1.4	1.3	1.3
<i>Improvement 3 / 4</i>					1.0	1.0	1.0	1.0	1.1	1.4	1.5	1.2	1.2
<i>Improvement 4 / 5</i>					1.1	0.9	1.0	0.9	1.2	1.0	1.2	1.2	1.1
<i>Improvement 6 / 5</i>					1.2	1.3	1.3	1.2	1.1	1.0	1.3	1.08	1.08

Table 2 Results of bundle adjustment and accuracy verification.

- AP.....Number of additional parameters
- Co.....Number of control points
- Ch.....Number of check points
- r.....Redundancy
- $\hat{\sigma}_0$ Variance of unit weight *a posteriori*
- $\hat{\sigma}_X, \hat{\sigma}_Y, \hat{\sigma}_Z$ Theoretical precision of check point coordinates
- μ_X, μ_Y, μ_Z Root Mean Square Error from comparison to check point coordinates in object space
- μ_x, μ_y Root Mean Square Error from comparison to check point coordinates in image space

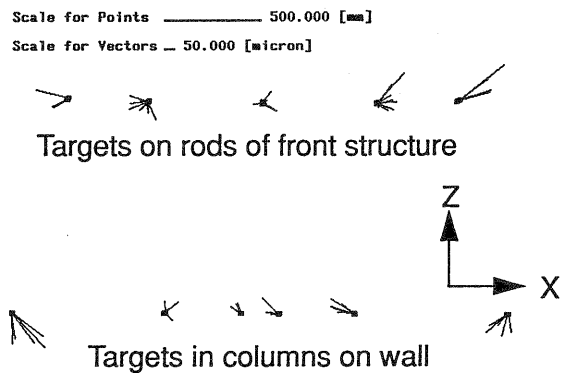


Figure 15 Differences to check points of version 5 (test-field as viewed from top).

The plots of checkpoint residuals of version 4 exhibit further systematic discrepancies which were traced. The small imaging scale and oblique imaging of targets on the rods of the testfield structure led to an influence of the (darker) background on the target area. This resulted in displacements comparable to those of local illumination gradients. Targets which were imaged too obliquely were eliminated for version 5. The relative precision of version 5 corresponds to 1 part in 100000 for both the X and Y axis. The relative accuracy is 1 part in 50000 for the same axes. The accuracy in image space corresponds to 1/85th of the pixel spacing. An accuracy of 1/50th of the pixel spacing can be attained when using a minimum datum only. This difference might appear large, but must be partially attributed to residual effects of local illumination gradients, which are partially absorbed when using more control points. These effects reached 0.03 pixel for the targets which were eliminated in the step from version 3 to 4 and are assumed to reach 0.02 pixel for other targets still in the data set. Systematic discrepancies can also be detected for targets in columns as shown in the plot of the differences to checkpoints in Figure 15. The overall accuracy improvement in image space attained by using a smaller template and eliminating targets with large degradations (version 2 to 5) is a factor of 1.8 and 1.7 in x and y.

3.4 Accuracy with PLL Line-Synchronization

The imagery was acquired at identical positions with pixel-synchronous sampling and PLL line-synchronization within 30 seconds of each other. It is thus possible to compare the effect of the synchronization on the three-dimensional accuracy under practically identical conditions. The image coordinates were again measured with LSM using a 5 x 5 template and the targets which were eliminated due to local illumination gradients and too oblique imaging conditions on the rods were removed from the data. Figure 16 shows a comparison of the image coordinates for 6 frames acquired at the left topmost station (see Figure 12). The average displacement between the two images of 0.125 and 1.988 pixel in x and y was removed before the plot. The average displacement in x was attributed to a difference in the sampling point and the difference in y was due to differences in the settings of the frame grabber for the selection of the active image region in vertical direction for the two acquisition modes (the determined value is only 0.002 pixel off the actual difference of 2 pixels). The large geometric deformation and instability (especially in x) of PLL line-synchronization is apparent from the figure. The RMS value of the

discrepancy is 0.1 pixel in x and 0.05 pixel in y. The results of the bundle adjustment (version 6 in Table 2) show that the accuracy is only slightly degraded as compared to that of pixelsynchronous frame grabbing. This close agreement of the results is attributable to the high degree of redundancy and indicates that the accuracy is limited by effects other than the synchronization. The shear determined by the additional parameters in the bundle adjustment is in good agreement with the values computed in the analysis of the frame grabber and of signal transmission.

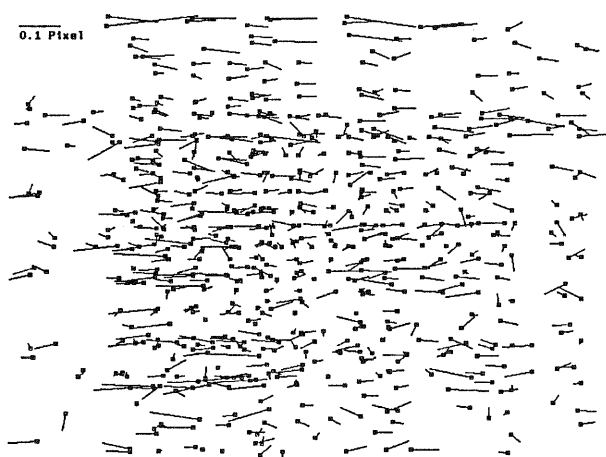


Figure 16 Differences of image coordinates between PLL line-synchronization and pixelsynchronous sampling for 6 frames.

The results of the two synchronization methods were further analyzed by using the object coordinates obtained in a version with minimum control and pixelsynchronous sampling as reference coordinates for a version of the PLL line-synchronization imagery with identical control. The RMS difference of the object space coordinates are 0.036, 0.033 and 0.044 mm in X, Y, and Z respectively. The accuracy in image space is 0.11 and 0.10 pixel in x and y respectively. This shows that an internal precision of three-dimensional measurements of 0.01 pixel can be attained when identical illumination and imaging conditions are present. The RMS differences correspond to 1 part in over 70000.

3.5 Limiting Factors

The theoretical precision estimates and the empirical accuracy measures of version 5 differ by a factor of 2 in X and Y and 1.5 in Z. Potential origins of this large difference were consequently investigated.

The precision of the reference coordinates is insufficient to verify this accuracy level. When correcting the theoretical precision estimates for the precision of the reference coordinates and the centricity of the targets used by the theodolite and CCD-cameras the difference to the empirical accuracy measures is decreased to factors of 1.6, 1.4, and 1.1 in X, Y, and Z respectively. It was already noted above that the comparison to the reference coordinates exhibit systematic differences (see Figure 16). These could at least in part be attributable to effects of smaller local illumination gradients. This was also found in other studies through slight variation of the illu-

mination conditions. The effects of the use of an affine transformation instead of a perspective transformation in LSM was also investigated. Considering that the average error will result in a shift it was concluded that the effect thereof can be neglected as compared to the influence of local illumination gradients. A further modelling with supplementary additional parameters (Brown, 1976 and Grün, 1978) was attempted but did not lead to any improvement.

It was thus concluded that the accuracy in this test was primarily limited by the local illumination gradients, the non-uniform background, the small image scale, and the large difference thereof. Local illumination gradients could be eliminated by the use of retro-reflective targets. The non-uniform background can be improved on by designing a larger area around the targets. The image scale/target size in the imagery, i.e. the number of pixels onto which a target is imaged, can be improved by using larger targets and/or a camera with higher "resolution". The first option is not always practical. The target diameter of 20 mm across a 2.6 m large object is already quite large for practical applications. This can in fact be improved with retro targets as their return is much better and scattering significantly increases the apparent diameter in the imagery. A high "resolution" camera, i.e. a camera delivering over 1024 x 1024 pixels, would also reduce the effects of local illumination gradients and non-uniform background as the area surrounding the target affecting the target localization is smaller. Finally the large variation of image scale could be reduced when using a longer focal length than the 9 mm lens used here due to space restrictions.

4 CONCLUSIONS

The radiometric and geometric characteristics of a number of elements involved in image acquisition with digital imaging system have been outlined and their effects on the accuracy of three-dimensional photogrammetric measurements discussed. A number of sources leading to potential degradations have been located. The performance of off-the-shelf equipment was demonstrated with a three-dimensional accuracy test. It could be shown that accuracies of $1/85^{\text{th}}$ of the pixel spacing can be attained. It was found that accuracies comparable to pixelsynchronous frame grabbing can be attained with PLL line-synchronization when a highly redundant network is used. The limitations indicate that even higher accuracies should be attainable under better environmental conditions as no limitations found so far are of a fundamental nature. It can thus be expected that accuracies approaching the $1/100^{\text{th}}$ of the pixel spacing can indeed be attained.

5 REFERENCES

- Beyer, H.A., 1988. Linejitter and Geometric Calibration of CCD-Cameras. *International Archives of Photogrammetry and Remote Sensing*, Vol. 27, Part B10, pp. 315-324. and in: *ISPRS Journal of Photogrammetry and Remote Sensing*, 45, 1990, pp. 17-32.

- Beyer, H.A., 1991. Evaluating the Geometric Performance of Signal Transmission, First Australian Photogrammetric Conference, 7 - 9 November 1991, Sydney, Australia.
- Beyer, H.A., 1992a. Geometric and Radiometric Analysis of a CCD-Camera based Photogrammetric Close-Range System. Dissertation No 9701, ETH-Zürich.
- Beyer, H.A., 1992b. An Introduction to Solid-State Sensors. In preparation.
- Blouke, M.M., Janesick, J.R., Elliott, T., Hall, J.E., Cowens, M.W., May, P.J., 1987. Current Status of the 800 x 800 Charge-Coupled-Device Image Sensor. OE, September 1987, Vol. 26 No. 9, pp. 864-874.
- Bösemann, W., Godding, R., Riechmann, W., 1990. Photogrammetric Investigation of CCD Cameras. SPIE Vol. 1395, pp. 119-126.
- Brown, D.C., 1976. The Bundle Adjustment - Progress and Prospects. IAP, Vol. XXI, Part 3, Invited Paper, Kommission III, ISP Congress, Helsinki.
- Burner, A.W., Snow, W.L., and Goad, W.K., 1985. Close Range Photogrammetry With Video Cameras. Technical Papers - 51st Annual Meeting ASP, Vol. 1, ASPRS, 62-77.
- Burner, A.W., Snow, W.L., Shortis, M.R., Goad, W.K., 1990. Laboratory Calibration and Characterization of Video Cameras. SPIE Vol. 1395, pp. 664-671.
- Curry, S., Baumrind, S., Anderson, J.M., 1986. Calibration of an Array Camera. PE&RS, Vol. 52, No. 5, pp. 627-636.
- Dähler, J., 1987. Problems in Digital Image Acquisition with CCD-Cameras. in: Proceedings of the ISPRS Intercommission Conference, Interlaken, pp.48-59.
- El-Hakim, S.F., 1986. A Real-Time System for Object Measurement with CCD cameras. IAPRS, Vol. 26, Part 5, pp. 363-373.
- Gruen, A., 1985. Adaptive least squares correlation - a powerful image matching technique. South African Journal of Photogrammetry, Remote Sensing and Cartography, 14 (3), pp. 175-187.
- Gruen, A.W., Beyer, H.A., 1986. Real-Time Photogrammetry at the Digital Photogrammetric Station (DIPS) of ETH Zurich. Paper presented at the ISPRS Commission V Symposium, "Real-Time Photogrammetry - A New Challenge", June 16-19, 1986, Ottawa, and in: The Canadian Surveyor, Vol. 41., No. 2, Summer 1987, pp. 181-199.
- Gustafson, P.C., 1991. An Accuracy/Repeatability Test for a Video Photogrammetric Measurement. SPIE Vol. 1526, Industrial Vision Metrology, pp. 36 - 41.
- Gülch, E., 1984. Geometric Calibration for two CCD-Cameras used for Digital Image Correlation on the Planicom C100. IAPRS, Vol. XXV, Part A3a, pp. 159-168.
- Gruen, A.W., 1978. Accuracy, Reliability and Statistics in Close-Range Photogrammetry. Presented paper, Inter-Congress Symposium, ISPRS Commission V, Stockholm, August 1978.
- Haggrén, H., 1984. New vistas for Industrial Photogrammetry. IAPRS, Vol. 25, Part A5, commission V, ISPRS Congress Rio de Janeiro, pp. 382-391.
- Haggrén, H., 1991. Real-Time Photogrammetry and Robot Vision. 43. Photogrammetrische Woche, Universität Stuttgart, 9-14. September 1991.
- Heikkilä, J., 1988. Some Tests on the Stability of the Digitization of analog Video Signal. Photogrammetric Journal of Finland, Vol. 11, No. 1, 1988, pp. 12-19.
- Lenz, R., 1988. Videometrie mit CCD-Sensoren und ihre Anwendung in der Robotik. Habilitationsschrift, Technische Universität München, München.
- Luhmann, T., 1988. Ein hochauflösendes automatisches Bildmeßsystem. Wissenschaftliche Arbeiten der Fachrichtung Vermessungswesen der Universität Hannover, Nr. 154, Hannover.
- Pinkney, H.F.L., 1978. Theory and Development of an On-Line 30 Hz Video Photogrammetric System for Real-Time 3-Dimensional Control. Proceedings of ISP Symposium on Photogrammetry for Industry, August, 1978, Stockholm.
- Raynor, J., Seitz, P., 1990. The Technology and Practical Problems of Pixel-Synchronous CCD Data Acquisition for Optical Metrology Applications. SPIE, Vol. 1395, 96-103.
- Shortis, M.R., Burner, A.W., Snow, W.L., Goad, W.K., 1991. Calibration Tests of Industrial and Scientific CCD Cameras. First Australian Photogrammetric Conference, 7 - 9 November 1991, Sydney, Australia.
- Wiley, A.G., Wong, K.W., 1990. Metric aspects of zoom vision. SPIE Vol. 1395, pp. 112-118.
- Wong, K.W. 1969. Geometric Distortions in Television Imagery. PE Vol. 35, No. 5, pp. 493-500.
- Wong, K.W., Ho, W.H., 1986. Close - Range Mapping with a Solid State Camera Photogrammetric Engineering and Remote Sensing, Vol. 52, no. 1, January 1986, pp. 67-74.